Article

Laser-Assisted Patterning of Co−Ni Alloy/Reduced Graphene Oxide Composite for Enhanced Micro-supercapacitor Performance

Jaemin Jung,[†] Jae Ryeol Jeong,[†] Cu Dang Van,[†] Kyungtae Kang, and Min Hyung Lee*

Cite This: ACS Appl. Electron. Mater. 2022, 4, 4840−4848

Read Online

ACCESS | Metrics & More | Article Recommendations | Supporting Information

ABSTRACT: The development of methods for the facile fabrication of complex micro-supercapacitors (MSCs) has drawn much attention owing to the increment in their use in wearable and flexible microscale electronics. In particular, interdigitated MSCs with pseudocapacitive behavior have been attractive as energy storage for small-scale devices, owing to their potential to achieve high power density and excellent cycling durability within a limited area. However, complicated and multiple patterning processes are required to assemble pseudocapacitive materials and electrodes in microscale interdigitated designs. Therefore, a fabrication method is required that can be used to produce interdigitated MSCs in a facile and single-step manner. In this work, the one-pot patterning of an interdigitated Co−Ni/reduced graphene oxide (rGO) composite on a flexible substrate is presented via the infrared (IR) laser scribing of a layered double hydroxide (LDH)/graphene oxide (GO) precursor film. Owing to the homogeneous distribution of transition metal nanoparticles (NPs) within the rGO, the patterned Co−Ni/rGO electrodes show excellent electrical conductivity compared to bare rGO, which contributes toward its increased power density. In addition, the Co−Ni/rGO MSCs exhibit increased energy density compared to that of rGO MSCs due to the pseudocapacitive behavior of well-dispersed Co−Ni NPs.

KEYWORDS: micro-supercapacitor, Co−Ni alloy, reduced graphene oxide, laser scribing, energy storage
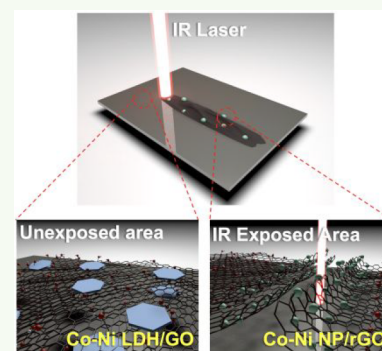
INTRODUCTION

Composites of metal or metal oxide NPs with graphene have been investigated as potential advanced materials for the electrodes of electronic devices and electrochemical devices. In particular, graphene composites have attracted a huge amount of interest for their application in energy storage devices, owing to their chemical and thermal durability, high surface area, and extraordinary conductivity.[1] Graphene with a high surface-area-to-volume ratio is an ideal platform for decoration with metal or metal oxide NPs to prevent them from agglomerating during electrochemical reactions.[2] This antiagglomeration function of graphene is good for maintaining the charge−discharge stability in energy storage devices. Redox materials, such as metal oxides and metal, can enhance the energy and power densities of supercapacitors by pseudocapacitance as a result of reversible surface redox reactions. To this aim, recently, there have been great efforts made to synthesize second-phase materials, including the compositing of various metals[2,3] and metal oxide NPs[2,4,5] with graphene. However, generally, these composites are synthesized via solution processes, therefore making it very difficult to apply such synthetic materials to planar MSCs, which require an additional patterning process to locate the composites on a desired area. Laser-assisted fabrication has been studied widely because it allows the direct synthesis of nanomaterials into microscale patterns without a photomask and can be applied in

supercapacitors,[6] batteries, and electrocatalysts.[7] In particular, the site-specific reduction of GO to highly conductive rGO has been used to fabricate flexible MSCs because of the local photothermal reaction under IR laser irradiation.[8,9] A previous study developed a laser-assisted ZnO nanorod (NR)/rGO patterning method.[10] However, the previous technique required the post-hydrothermal growth of the ZnO NRs after a laser-assisted ZnO seed formation process. For a more convenient and facile fabrication of MSCs comprising second-phase materials, it is thus desirable to achieve the one-pot synthesis of metal/rGO composites on patterned areas using a laser scribing process.

Herein, a one-pot synthesis of Co−Ni/rGO in a patterned design via laser scanning and the fabrication of interdigitated MSCs on a flexible poly(ethylene terephthalate) (PET) is described. When a Co−Ni LDH is introduced as a metal precursor and its binding interaction is tuned with GO, well-dispersed Co−Ni metal particles in rGO were obtained after laser scanning, resulting in the prepared MSCs exhibiting
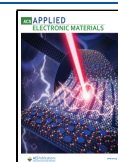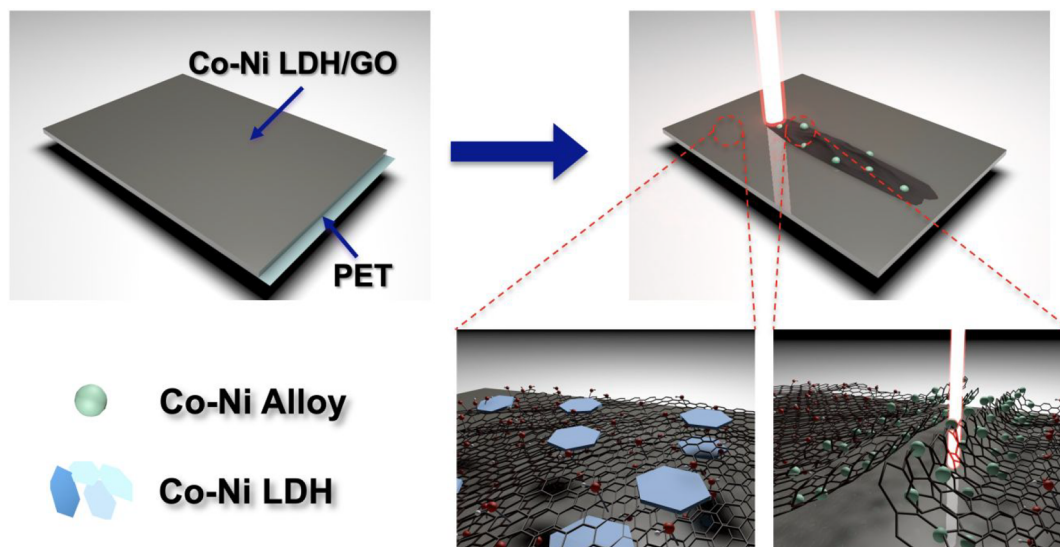
Figure 1. Schematic illustration of the fabrication process of an MSC based on Co−Ni/rGO composites on PET. A Co−Ni LDH/GO film is formed by drop casting on PET followed by the photothermal conversion of the Co−Ni LDH/GO precursors into Co−Ni NPs/rGO after IR-laser scanning.

optimum capacitive performance. Compared to our previous work on ZnO NR/rGO patterning, the Co−Ni/rGO electrodes in this work exhibit high electrical conductivity, contributing to the formation of an MSC with drastically enhanced power and energy densities. The Co−Ni/rGO MSC shows a stack capacitance of 5.50 F cm^{-3}, a power density of 0.54 W cm^{-3}, and an energy density of 0.63 mWh cm^{-3} that are around four times higher than those of a pristine rGO MSC.

RESULTS AND DISCUSSION

Fabrication of the Co−Ni/rGO Pattern. The process of fabricating the MSC using the Co−Ni/rGO composite as an active material is shown in Figure 1. In brief, a homogeneous coating of Co−Ni LDH/GO was formed on the PET film via drop casting of the Co−Ni LDH/GO precursor in water. After that, an MSC with an interdigitated electrode design was patterned via the photothermal reduction of the precursor using an IR laser integrated into a LightScribe DVD recorder. First, a solution of GO was prepared via the synthetic process described in our previous report.[11] Careful preparation of a well-dispersed Co−Ni LDH/GO precursor is important to form a homogeneous film of the Co−Ni LDH/GO composite on PET. Oxygenated defects on GO sheets can be categorized into two groups on the basis of their geometric conditions: (i) basal planes functionalized with epoxide and hydroxyl groups and (ii) edge sites with carboxylic acid moieties.[12] To stabilize GO nanosheets in water, an electrostatic repulsive force between the GO sheets needs to overcome the van der Waals interactions. It is well-known that ionization of carboxylic groups at the edge sites in GO plays a pivotal role in the electrostatic repulsion of GO nanosheets, which has been confirmed by the aggregation of the GO sheets due to nonionized carboxylic acid groups in a low pH environment.[13,14] Thus, the maintenance of the carboxylic functional groups at the edge sites of GO sheets during the synthesis of the Co−Ni LDH is critical to obtaining a stable colloidal Co−Ni LDH/GO solution. Therefore, to maintain the carboxylic acid groups, the ratio of the Co−Ni LDH source and GO was

modulated to guide the required amount of Co−Ni LDH growth on the basal planes instead of at the edge sites of the GO sheets. At a Co−Ni LDH/GO mass ratio of 5:1, the Co−Ni LDH colloids become aggregated because there is an excess of Co−Ni LDH, more than enough to screen the negative charges of the carboxylate groups at the edge sites of the GO sheets. However, at a Co−Ni LDH/GO mass ratio of 1:1, the Co−Ni LDH/GO colloids are well-dispersed due to the presence of carboxyl moieties at the edge sites of the GO. Thus, a Co−Ni LDH/GO mass ratio of 1:1 of the Co−Ni LDH/GO precursor solution is appropriate to form a homogeneous Co−Ni LDH/GO film via drop casting it on a PET substrate (Figure S1). Next, the as-prepared Co−Ni LDH/GO film on PET was exposed to the scanned illumination of an IR laser with repeated scanning for three times to fabricate the Co−Ni/rGO MSC electrode. During the IR-laser scanning, GO is converted into rGO via the photothermal deoxygenation of GO[15] with the Co−Ni LDH being simultaneously converted into a Co−Ni alloy due to an increase in its local temperature of up to ∼1000 °C.[16] As previously reported, a volumetric increase in rGO was observed due to the deoxygenation process, resulting in enhanced capacitance with a high surface-to-volume ratio.[17] Unlike pristine rGO, the degree of the volume expansion of the rGO sheets decreased due to the interactions of the Co−Ni metal with the oxygen groups of the basal planes of the GO.[18] Furthermore, an electrostatic attractive force between the positively charged Co−Ni LDH and negatively charged GO surface can be ascribed to the decrease in the degree of the volume expansion of the rGO.[19] Although the degree of swelling between the graphene layers decreases, the gap between the Co−Ni/rGO layers is still large enough to allow ions to exchange in the electrolyte toward the operation of the MSC.

Analysis of the Co−Ni/rGO Composite. To examine the conversion of the material during the laser scribing process, electron microscopy analyses were performed on a Co−Ni/rGO composite film after IR-laser scanning. A thin layer of the Co−Ni LDH can be observed on the GO sheets in the TEM
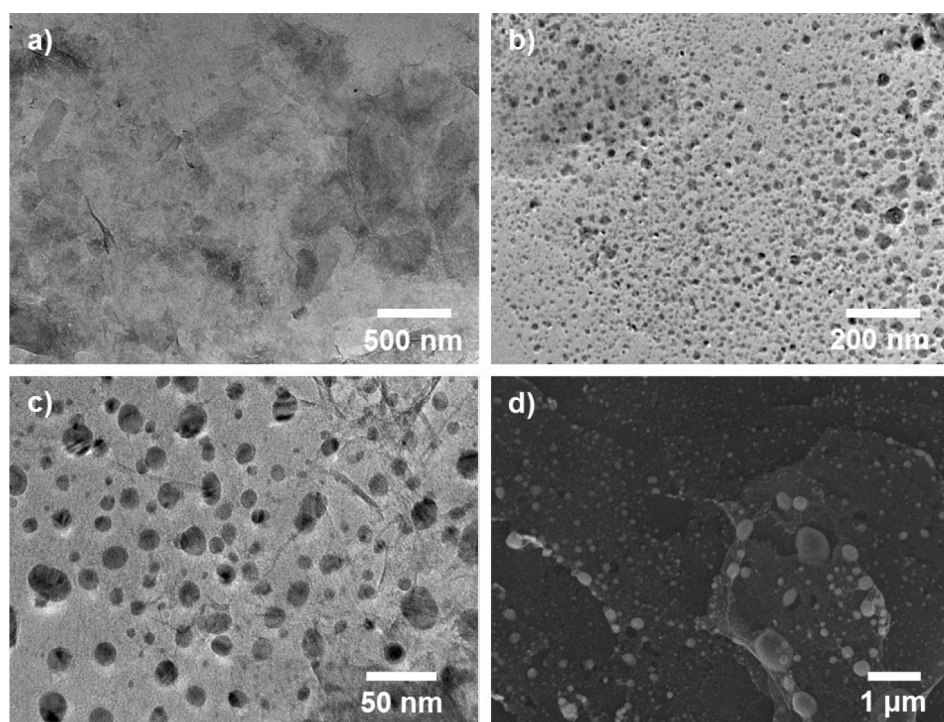
Figure 2. TEM images taken from areas (a) unexposed (i.e., Co−Ni LDH/GO film) and (b, c) exposed (i.e., Co−Ni NPs/rGO) to an IR laser. (d) SEM image of the film subjected to IR-laser scribing.
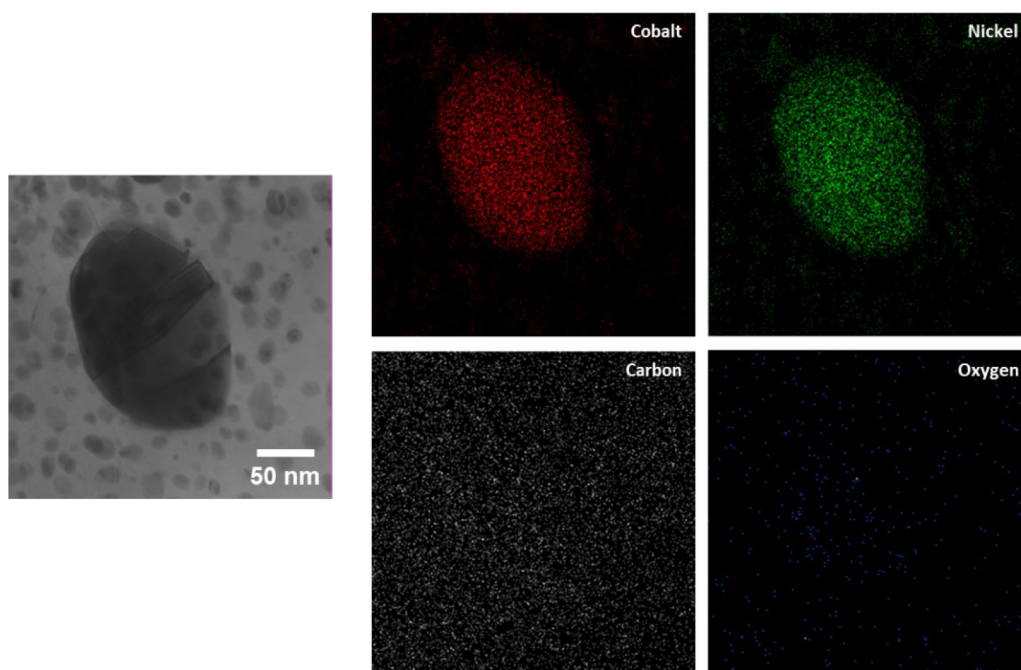

Figure 3. EDX spectroscopy mapping results of the Co−Ni/rGO composite focused on a Co−Ni NP, where Co and Ni were found to be the main components.

image of the area not exposed to the IR laser (Figure 2a). The Co−Ni LDH and the GO sheets are in the form of two-dimensional (2D) sheets without any observable particle formation, reflecting that a localized photothermal conversion process occurs during their laser scanning. However, a high density of spherical Co−Ni NPs is observed on the rGO sheets subjected to an IR laser, confirming the successful photo-thermal conversion of Co−Ni LDH into Co−Ni NPs (with a

median diameter of ca. 9.88 nm, Figure S2) after the IR-laser scribing process (Figure 2b−c). In addition, the uniform distribution of Co−Ni alloy NPs over the entire surface of the rGO sheets can be observed in the scanning electron microscopy (SEM) image of Co−Ni/rGO (Figure 2d). Figure S3 shows cross-section SEM images of rGO and Co−Ni/rGO. After laser scribing, the rGO layers became thicker than the GO layers, indicating an increased volume of rGO due to laser-
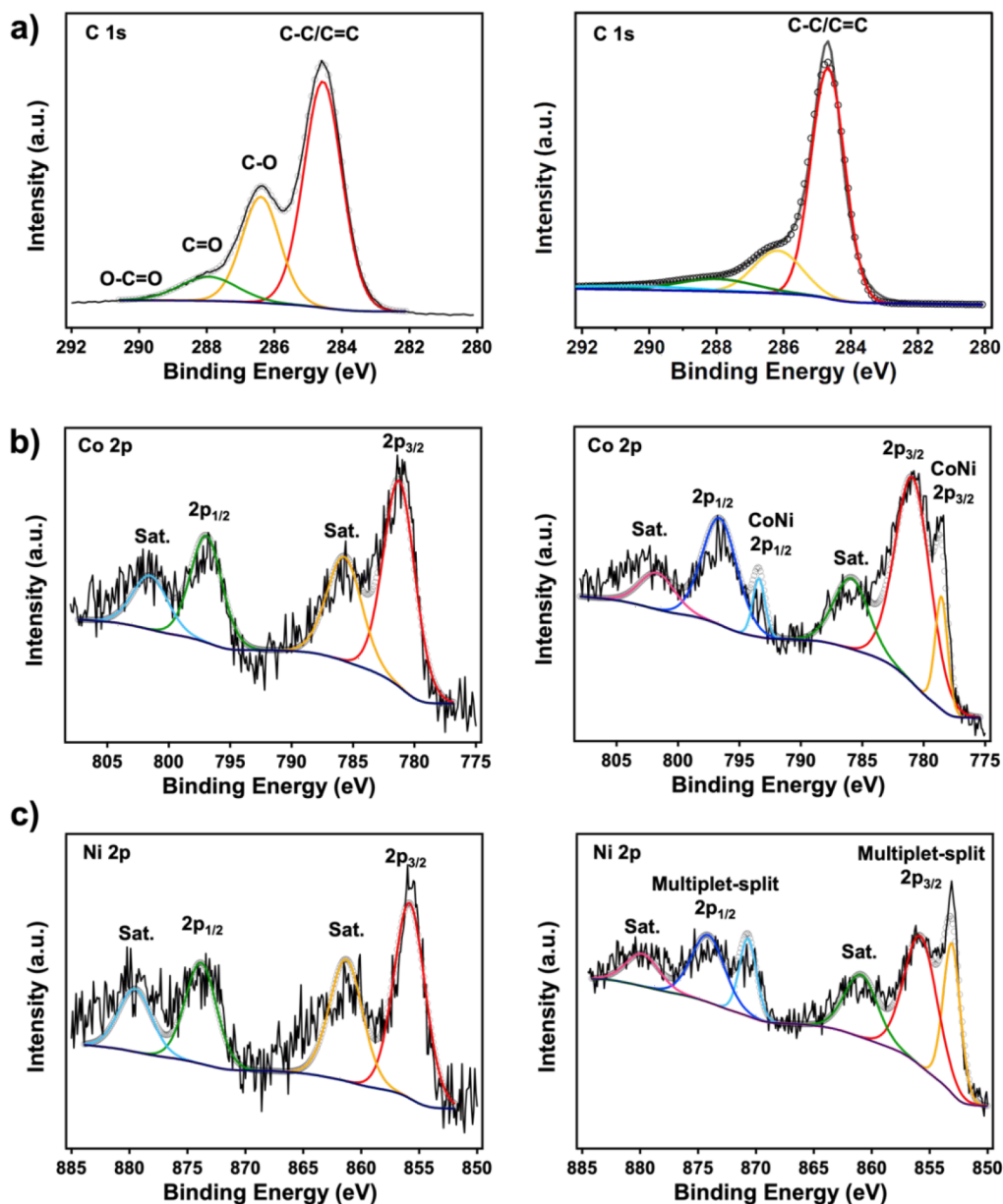
Figure 4. Changes in the (a) C 1s, (b) Co 2p, and (c) Ni 2p XPS data before (left column) and after (right column) IR-laser scanning of the Co–Ni LDH/GO film.

induced Joule heating on the local film and the gasification of oxygen species (Figure S3a). Stacked graphene layers were observed in the high magnification SEM images. Even after the introduction of the Co–Ni alloy, the Co–Ni/rGO film did not show any remarkable change in the cross-section rGO morphology compared to the pristine rGO film (Figure S3b). The porous structure with the stacked rGO layers can facilitate the wetting by the electrolyte and the ion diffusion during the charging–discharging processes of the MSCs. In our previous report, ZnO NR/rGO composites were synthesized by the combination of ZnO seed formation via IR-laser scanning and seed-mediated growth of ZnO NRs.[10] However, the two-step method led to the formation of ZnO NRs on the rGO, but the post-hydrothermal ZnO growth step could cause a decrease in porosity of rGO due to the restacking between rGO sheets by the hydrogen bonding of intercalated water.[20] In contrast, the one-pot synthesis method reported herein can lead to the homogeneous distribution of active

materials in MSCs, such as metals or metal oxide NPs, without losing the porosity of rGO, which has a positive contribution on the electrochemical process by improving the electron and ion transfer.

To confirm the crystallinity of the Co–Ni NPs, high-resolution transmission electron microscopy (HRTEM) images were recorded (Figure S4), where even ca. 4 nm-scale diameter NPs show an ordered crystalline lattice with a lattice distance of ∼0.2 nm, indicating the effective formation of Co–Ni NPs via the laser scanning process (Figure S4a). The smaller the Co–Ni NPs on the rGO, the higher is the surface area in a given volume, promising increased Faradaic capacitance of the MSC via the redox reactions of the active materials.[21] Figure S4b presents the selected area electron diffraction (SAED) patterns of the Co–Ni/rGO composites. Two diffuse diffraction rings corresponding to polycrystalline rGO sheets and a randomly distributed dot pattern corresponding to crystalline Co–Ni NPs can be observed in
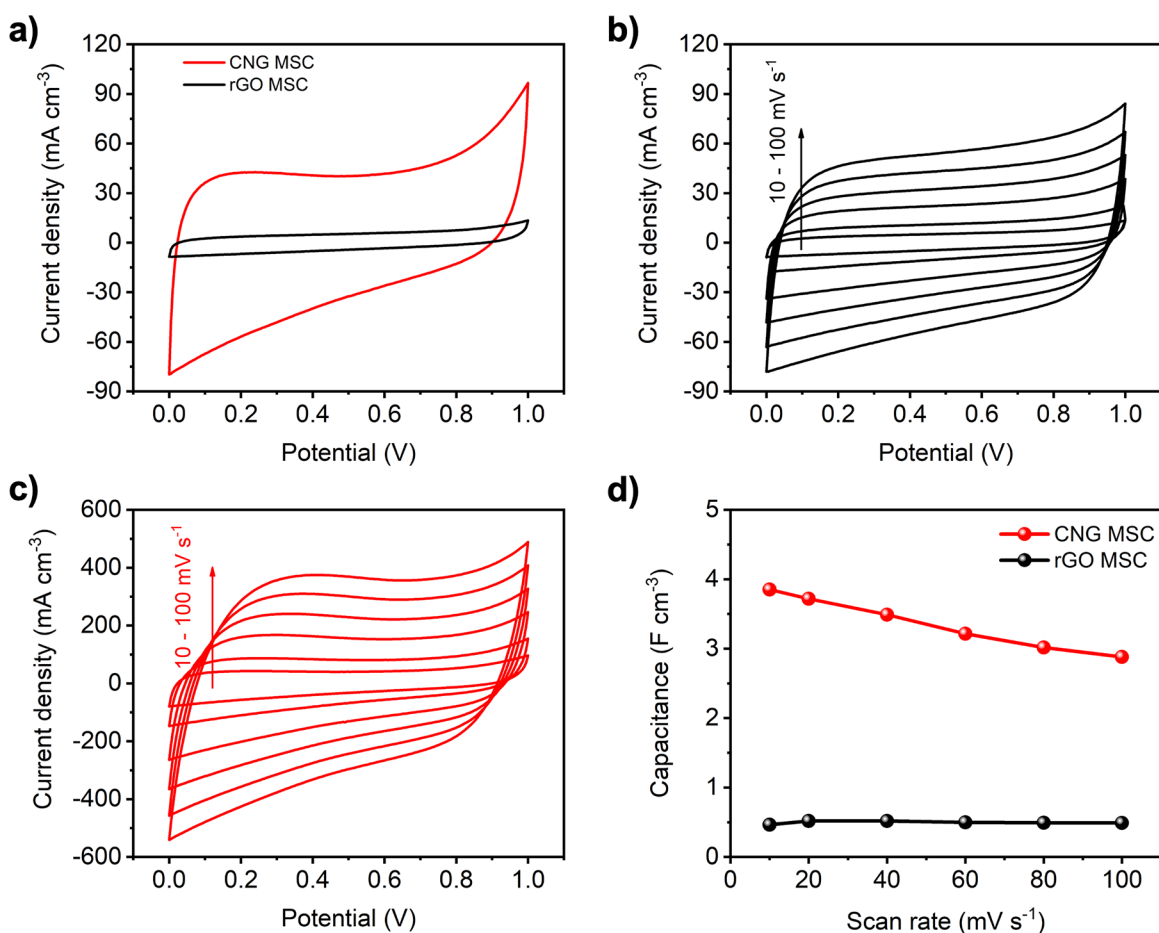
Figure 5. (a) CV curves of the CNG MSC (red) and rGO MSC (black) at a scan rate of 10 mV s^{-1}. CV curves recorded at different scan rates for (b) rGO MSC and (c) CNG MSC. (d) Capacitances of CNG MSC (red) and rGO MSC (black) recorded at different scan rates.

the SAED patterns of Co−Ni NPs/rGO, confirming the Co−Ni NP/rGO composite formation via the IR-laser scribing method. Furthermore, the X-ray diffraction (XRD) pattern in Figure S5 further confirmed the introduction of the (002) plane of rGO (blue peak) and the planes of (111) and (200) for the Co−Ni alloy (red peaks) in the Co−Ni NP/rGO composite.

To investigate the chemical species of the NPs, energy-dispersive X-ray (EDX) spectroscopy mapping was performed, and the results are presented in Figure 3. EDX data are collected from relatively large particles to allow accurate component analysis. The homogeneous distribution of Co and Ni across the entirety of the NP area is observed with high intensity and medium intensity for C and a very low O signal over the entire region, indicating the simultaneous formation of the Co−Ni NPs and highly reduced GO with minor O-moieties via the one-pot laser scanning of the Co−Ni LDH/GO film. Compared to an electric double layer capacitor (EDLC), capacitive performance can be improved by employing the simple fabrication of Co−Ni NP alloys that promote redox reactions on the surface during the charge−discharge processes.[2,17]

To further investigate the chemical compositional changes that occur during the fabrication of the materials, X-ray photoelectron spectroscopy (XPS) measurements were conducted before and after their IR-laser treatment. In the C 1s XPS data, most peaks associated with the O-functional groups of GO can no longer be observed, and only C−C/C=C bonds

remain, indicating the successful formation of rGO via the IR-laser-assisted photothermal reduction (Figure 4a). Unlike the conventional C 1s XPS data of GO, the relative peak intensity of the C−O is far lower than that of the C−C/C=C peak. This XPS trend can be ascribed to the binding of metal ions to the O-groups of GO, indirectly proving the well-organized formation of the Co−Ni LDH on the GO sheets.[18] In agreement with the C 1s spectra, two distinct Co XPS peaks for $2p_{1/2}$ and $2p_{3/2}$ and two satellite peaks for each of the 2p peaks can be observed before the laser scribing of the material, indicating that Co is in its hydroxide form (Co−Ni LDH) (Figure 4b).[22] After laser treatment, the main peaks of Co 2p are separated into a multiplet (the peaks at 780.48 and 793.00 eV) corresponding to a Co−Ni alloy with a similar trend in the Co−Ni binding XPS peaks also being observed for the XPS of Ni 2p (Figure 4c).[23] Overall, the XPS analyses confirm the successful transformation of the Co−Ni LDH/GO film into a Co−Ni NPs/rGO composite via the simultaneous photo-thermal reduction of Co−Ni LDH and GO. Furthermore, a drastic change is observed in the overall binding energy peak ratio of O and C after the laser scanning process (Figure S6). Before the laser treatment, the C 1s and O 1s peaks have similar intensities, but the C 1s peak intensity greatly increases and that of the O 1s peak decreases after laser treatment. This is a good indication that the GO has been reduced and that the O atoms bound to the metal in its hydroxide form have also been simultaneously reduced.
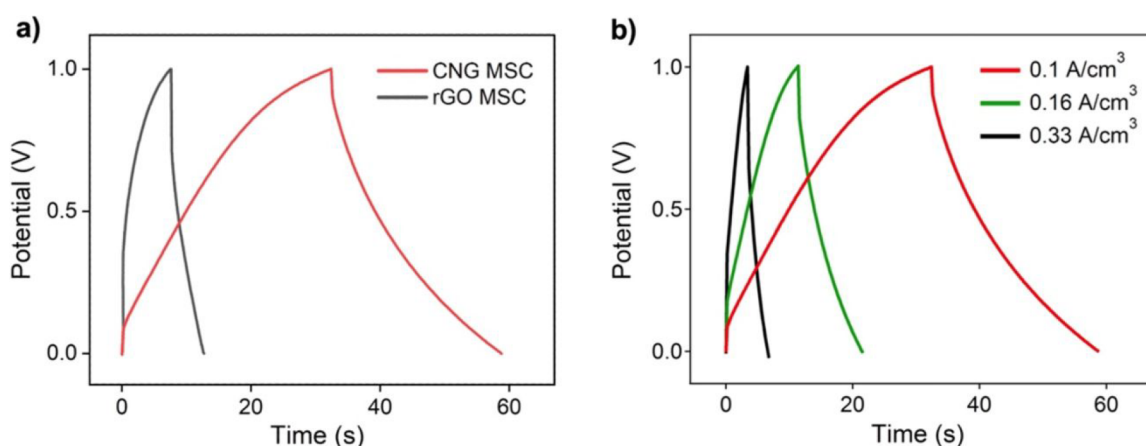
Figure 6. (a) GCD curves of the CNG MSC (red) and rGO MSC (black) recorded at a current density of 0.1 A cm^{-3}. (b) GCD curves of the CNG MSC recorded at different current densities.

Application of Planar MSCs. The Co−Ni NPs/rGO synthesis method was applied to fabricate planar MSCs by laser scanning along the predesigned interdigitated electrodes, as described in our previous report.[11] In the interdigitated electrodes of the MSCs, the active materials and conductive electrodes are composed of Co−Ni NPs/rGO produced by IR-laser-assisted photothermal reduction, and the separators are based on Co−Ni LDH/GO. Co−Ni LDH is located on GO and has very low conductivity; therefore, it is electrically insulated and does not participate in the electrochemical reaction. Solid-state H$_2$SO$_4$/PVA electrolyte was applied on the MSCs, and tests were performed under ambient environments. The electrochemical performance of Co−Ni NPs/rGO MSC (CNG MSC) was compared to a bare rGO MSC with the same design (Figure S7).

To investigate the pseudocapacitive effect of Co−Ni NPs in the CNG MSC, the capacitive behaviors of rGO MSC and CNG MSC were compared by conducting cyclic voltammetry (CV) measurements (Figure 5). Figure 5a shows the CV curves of rGO MSC and CNG MSC recorded at 10 mV s^{-1}. While the rGO MSC shows an almost rectangular shape, indicating its EDLC behavior, the CNG MSC presents a slightly distorted rectangular-shaped signal with a broad peak at 0−0.4 V, demonstrating its mixed EDLC and pseudocapacitive characteristic.[24,25] The EDLC of the rGO MSC mainly originates from its porous nature and large surface area of the rGO, which facilitates the adsorption/desorption of the ion species of the electrolyte.[26] Besides the EDLC behavior of the rGO, the CNG MSC with uniform Co−Ni alloy NPs shows pseudocapacitance via a reversible Faradaic redox reaction that occurs between the metal and electrolyte ions.[27] However, the CNG MSC also shows a rectangular CV curve similar to that of the rGO MSC, indicating its much reduced ohmic behavior due to the highly conductive Co−Ni/rGO composite. In our previous studies, MSCs were fabricated from ZnO NR/rGO (ZG MSCs) composites that show elliptical CV curves due to the ohmic behavior of the resistive ZnO NRs.[28] In terms of the conductivity of the active materials, the contact geometry between the active materials and rGO plays a pivotal role in the performance of the MSCs. Since one-dimensional (1D) ZnO NRs grow normal to the rGO sheets, there is only a small interfacial contact area (initial contact area of the ZnO seeds to rGO) with the rGO electrodes, limiting electron transfer and slowing the charge−discharge process. Compared to that, the good interfacial contact of the 2D Co−Ni LDH with 2D GO facilitates the homogeneous distribution of the Co−Ni NPs in rGO, resulting in facilitated electron migration through conductive rGO, thus boosting the charge−discharge process. Moreover, the CNG MSC exhibits a much wider integral area under its CV curve compared to that of the rGO MSC, indicating a larger stack capacitance of the CNG MSC. The electrochemical performances of the rGO MSC and CNG MSC were further investigated at different scan speeds, and the results are presented in Figure 5b,c. The shapes of the CV curves of the CNG MSC were maintained at a high scan speed of 100 mV s^{-1}, suggesting its fast charge−discharge performance with great power density.[29] The capacitances of each MSC were evaluated from their CV curves, and the results are presented in Figure 5d. The CNG MSC achieved a capacitance of 3.85 F cm^{-3}, which is 8.36 times larger than that of the rGO MSC at a 10 mV s^{-1}, and maintained a capacitance of 2.88 F cm^{-3} even up to a scan speed of 100 mV s^{-1}.

Figure 6a presents a comparison of the galvanostatic charge−discharge (GCD) curves of the pristine rGO MSC and CNG MSC, recorded at 0.1 A cm^{-3}. It can be clearly seen that the GCD curve of the CNG MSC is much wider than that of the rGO MSC and has a more linear charge−discharge curve, reflecting ideal capacitance behavior. These linear curves reflect that charge transfer resistance is relatively lower and that the charge−discharge mechanism is as fast as an electric double layer formation.[30] Since the Co−Ni NPs are small and have a high surface area, the Faradaic reaction occurs rapidly on their surface, resulting in a rapid charge−discharge process. In contrast, the GCD curve of the MSCs with the ZnO NRs as an active material is bent in shape, which is evidence of a slow Faradaic reaction and shows that it is hard to achieve fast charging and discharging due to the normal directional interfacial contact of the 1D ZnO NRs and 2D rGO electrodes.[28] Then, supercapacity values were extracted from the charge−discharge data with a stack capacitance of 5.50 F cm^{-3}, a power density of 0.54 W cm^{-3}, and an energy density of 0.63 mWh cm^{-3} measured for the CNG MSC. These results are around four times larger than those of the bare rGO MSC (with a stack capacitance of 1.44 F cm^{-3}, a power density of 0.29 W cm^{-3}, and an energy density of 0.15 mWh cm^{-3}) and around 1.4 times larger than those of the ZG MSCs reported in our previous work.[10]

To evaluate its practical applications, the GCD curves of the CNG MSC were collected at various current densities (0.1, 0.16, and 0.33 A cm^{-3}), and the results are presented in Figure 6b. All of the GCD curves are almost triangular in shape, demonstrating that the CNG MSC can operate across a broad range of current densities. Furthermore, its iR drop was still small even when operated at a high current density of 0.33 A cm^{-3}, confirming the high conductivity of the CNG MSC. In addition, the stack capacitances of the CNG MSC reached values of 3.70 and 3.10 F cm^{-3} at current densities of 0.16 and 0.33 A cm^{-3}, respectively. The performance of the CNG MSC was also compared with those of other reported MSCs by examining their Ragone plots (Figure S8). Through the comparison, it can be seen that the CNG MSC delivers high power and energy densities that are comparable to those of other reported MSCs.[31−37]

The improvement of the capacitive performance of the CNG MSC was examined further by electrochemical impedance spectroscopy (EIS) from 100 kHz to 0.01 Hz at 0.25 V. The lower x-intercept of the Nyquist showed that the CNG MSC had lower equivalent series resistance, suggesting that CNG MSC has higher conductivity than rGO MSC because of the introduction of Co−Ni alloy NPs in the composite (Figure S9a). In addition, the Bode plots for both MSCs in Figure S9b showed that the phase angle for CNG MSC was −74° at 10 mHz, which was closer to −90° for an ideal capacitor than that of rGO MSC (−71°). Moreover, the relaxation time corresponding to the phase angle of −45° of the CNG MSC (1 s) was three times shorter than that of rGO MSC (3 s), meaning that CNG MSC requires a shorter time to deliver 50% of the power than rGO MSC.

Finally, the long-term durability of CNG MSC was evaluated by CV at 30 mV s^{-1} for 3000 cycles (Figure S9c). Impressively, the capacitance increased 1.5-fold for the first 1000 cycles and then gradually decreased to 90% capacitance retention after 3000 cycles, highlighting the advantage of this design in MSCs.

■ CONCLUSIONS

In conclusion, a facile, selective, one-pot synthesis, and patterning method of a Co−Ni NP/rGO composite from a Co−Ni LDH/GO precursor has been successfully developed and applied to fabricate a planar MSC. Laser scribing of a Co−Ni LDH/GO composite film creates small and crystalline Co−Ni alloy particles that homogeneously distribute between rGO sheets. On account of the uniform distribution of small Co−Ni NPs on rGO, the resultant CNG MSC shows ∼400% enhanced capacitance compared to that of a pristine rGO MSC. Fast charging−discharging and high energy and power densities were achieved owing to the increased surface area and good interfacial contact between the Co−Ni NPs and rGO electrodes, resulting in effective redox reactions and fast electron transfer. Until now, the selective growth of active materials on conductive electrodes via a one-pot synthesis has rarely been reported; however, this laser-assisted fabrication technique makes it possible to fabricate metal and metal-oxide-based electrochemical devices in a simple manner.

■ EXPERIMENTAL SECTION

Synthesis of GO. GO was prepared using graphite flakes via the synthetic process described in detail in our previous report.[11]

Synthesis of the Co−Ni/rGO Composite and Fabrication of the Co−Ni/rGO MSC. *Synthesis of Colloidal Co−Ni LDH/GO.* The as-synthesized GO was used to prepare a 2.0 mg mL^{-1} aqueous GO

dispersion. To the prepared GO solution (15 mL), sodium hydroxide (NaOH, 15 mg, molecular weight (M.W.) 40.00, 97.0+%, Daejung) and sodium carbonate (Na$_2$CO$_3$, 6.5 mg, M.W. 105.99, 99.0%, Daejung) were added, and the resultant mixture was stirred to achieve a homogeneous solution. To this solution, nickel nitrate hexahydrate (Ni(NO$_3$)$_2$·6H$_2$O, 16.5 mg, M.W. 290.80, 99.99%, Alfa Aesar) and cobalt chloride hexahydrate (CoCl$_2$·6H$_2$O, 13.5 mg, M.W. 237.93, Sigma-Aldrich) were then added. Growth of the metal hydroxide was then enabled by maintaining the mixture at 60 °C for 6 h, followed by cooling the mixture to room temperature before being washed with DI water.

Patterning of the Co−Ni/rGO Composite. The PET was cut into a disc shape with the size of a DVD for use in a DVD recorder with a LightScribing function and attached to the disc using spray glue. Next, the as-prepared Co−Ni LDH/GO solution (20 mL) was coated onto the prepared PET film, which was then allowed to dry overnight. The prepared Co−Ni LDH/GO film on the PET/DVD was scanned using an integrated IR laser of a LightScribe DVD recorder (HP-337s, Hewlett-Packard) with predesigned interdigitated electrodes using bundled imaging software with the laser scribing process conducted three times.

Preparation of the H$_2$SO$_4$/PVA Gel Electrolyte. The H$_2$SO$_4$/PVA gel electrolyte was prepared as described in our previous report.[10]

Fabrication of a CNG MSC. The as-prepared H$_2$SO$_4$/PVA gel electrolyte was dropped onto the crossing area of the interdigitated electrodes of the CNG MSC; then, the gel electrolyte was dried overnight under room temperature to remove the excess water from the gel electrolyte. Next, the current collector was covered with silver paste (Elcoat p-100, CANS) for electrical contact with the probes of the electrochemical workstation without damaging on the rGO electrodes.

Characterization and Measurements. *Material Characterization.* The morphologies, crystallinities, and chemical compositions of synthesized materials were investigated by field-emission scanning electron microscopy (FESEM; LEO SUPRA 55, ZEISS), HRTEM (JEM-2100 F operated at 200 kV, JEOL), XRD (D8 Advance spectrometer equipped with a Cu Kα radiation source, Bruker), and XPS (K-Alpha spectrometer, Thermo Scientific). All of the XPS data were calibrated to the binding energy of the C 1s peak at 284.6 eV.

Electrochemical Measurements. The electrochemical evaluation of the MSCs was examined by conducting CV and GCD measurements, which were performed on a potentiostat instrument (IVIUMSTAT, Ivium technologies). The EIS measurements were conducted using a potentiostat (SP-200, BioLogic).

Calculations. Capacitance values were calculated from the CV curves recorded at various scan speeds using the following equation:

$$C = \frac{1}{2\upsilon V} \int i \, dV \tag{1}$$

where C (F) is the total capacitance contribution from the MSC, υ is the scan rate (V s^{-1}), and V (V) is the potential window.

The total capacitance (C_T), volumetric stack capacitance (C_{stack}), power density (P), energy density (E), and internal resistance (R_{ESR}) of the MSCs were calculated according to the methods described in our previous report.[10]

■ ASSOCIATED CONTENT

ⓈI Supporting Information

The Supporting Information is available free of charge at https://pubs.acs.org/doi/10.1021/acsaelm.2c00702.

Photograph of Co−Ni LDH/GO colloids depending on Co−Ni LDH/GO mass ratio, diameter distribution of Co−Ni NPs in CNG MSC, cross-sectional morphology of rGO MSC and CNG MSC, HRTEM image and SAED patterns of Co−Ni/rGO composites, XRD pattern of Co−Ni/rGO, XPS spectra of O 1s and C 1s of Co−Ni/rGO and Co−Ni LDH/GO, fabricated interdigitated CNG MSC on PET substrates, Ragone

plots that are based on volumetric energy and power densities of CNG MSC, Nyquist and Bode plots of the CNG MSC and rGO MSC, and cycling stability of CNG MSC (PDF)

■ AUTHOR INFORMATION

Corresponding Author

Min Hyung Lee − *Department of Applied Chemistry, Kyung Hee University, Yongin, Gyeonggi 17104, Korea;* orcid.org/0000-0001-8313-9857; Email: minhlee@ khu.ac.kr

Authors

Jaemin Jung − *Department of Applied Chemistry, Kyung Hee University, Yongin, Gyeonggi 17104, Korea;* orcid.org/ 0000-0002-8006-245X

Jae Ryeol Jeong − *Department of Applied Chemistry, Kyung Hee University, Yongin, Gyeonggi 17104, Korea;* orcid.org/0000-0002-3410-4321

Cu Dang Van − *Department of Applied Chemistry, Kyung Hee University, Yongin, Gyeonggi 17104, Korea;* orcid.org/ 0000-0003-3613-5399

Kyungtae Kang − *Department of Applied Chemistry, Kyung Hee University, Yongin, Gyeonggi 17104, Korea;* orcid.org/0000-0003-4236-8922

Complete contact information is available at:
https://pubs.acs.org/10.1021/acsaelm.2c00702

Author Contributions

[†]J.J., J.R.J., and C.D.V. contributed equally to this work.

Notes

The authors declare no competing financial interest.

■ REFERENCES

(1) Pumera, M. Graphene-Based Nanomaterials and Their Electrochemistry. *Chem. Soc. Rev.* **2010**, *39*, 4146−4157.

(2) Dong, X.; Cao, Y.; Wang, J.; Chan-Park, M. B.; Wang, L.; Huang, W.; Chen, P. Hybrid Structure of Zinc Oxide Nanorods and Three Dimensional Graphene Foam for Supercapacitor and Electrochemical Sensor Applications. *RSC Adv.* **2012**, *2*, 4364−4369.

(3) Ji, L.; Tan, Z.; Kuykendall, T.; An, E. J.; Fu, Y.; Battaglia, V.; Zhang, Y. Multilayer Nanoassembly of Sn-Nanopillar Arrays Sandwiched between Graphene Layers for High-Capacity Lithium Storage. *Energy Environ. Sci.* **2011**, *4*, 3611−3616.

(4) Yan, J.; Fan, Z.; Wei, T.; Qian, W.; Zhang, M.; Wei, F. Fast and Reversible Surface Redox Reaction of Graphene−MnO2 Composites as Supercapacitor Electrodes. *Carbon* **2010**, *48*, 3825−3833.

(5) Gilje, S.; Dubin, S.; Badakhshan, A.; Farrar, J.; Danczyk, S. A.; Kaner, R. B. Photothermal Deoxygenation of Graphene Oxide for Patterning and Distributed Ignition Applications. *Adv. Mater.* **2010**, *22*, 419−423.

(6) Wang, Y.; Zhao, Y.; Qu, L. Laser Fabrication of Functional Micro-Supercapacitors. *J. Energy Chem.* **2021**, *59*, 642−665.

(7) Zhao, L.; Liu, Z.; Chen, D.; Liu, F.; Yang, Z.; Li, X.; Yu, H.; Liu, H.; Zhou, W. Laser Synthesis and Microfabrication of Micro/ Nanostructured Materials toward Energy Conversion and Storage. *Nanomicro Lett.* **2021**, *13*, 49.

(8) Kirubasankar, B.; Balan, B.; Yan, C.; Angaiah, S. Recent Progress in Graphene-Based Microsupercapacitors. *Energy Technol.* **2021**, *9*, 2000844.

(9) Li, L.; Hu, C.; Liu, W.; Shen, G. Progress and Perspectives in Designing Flexible Microsupercapacitors. *Micromachines* **2021**, *12*, 1305.

(10) Jung, J.; Jeong, J. R.; Lee, J.; Lee, S. H.; Kim, S. Y.; Kim, M. J.; Nah, J.; Lee, M. H. In Situ Formation of Graphene/Metal Oxide Composites for High-Energy Microsupercapacitors. *NPG Asia Mater.* **2020**, *12*, 50.

(11) Lee, S. H.; Lee, J.; Jung, J.; Cho, A. R.; Jeong, J. R.; Dang Van, C.; Nah, J.; Lee, M. H. Enhanced Electrochemical Performance of Micro-Supercapacitors via Laser-Scribed Cobalt/Reduced Graphene Oxide Hybrids. *ACS Appl. Mater. Interfaces* **2021**, *13*, 18821−18828.

(12) Hummers, W. S.; Offeman, R. E. Preparation of Graphitic Oxide. *J. Am. Chem. Soc.* **1958**, *80*, 1339−1339.

(13) Shih, C. J.; Lin, S.; Sharma, R.; Strano, M. S.; Blankschtein, D. Understanding the pH-Dependent Behavior of Graphene Oxide Aqueous Solutions: A Comparative Experimental and Molecular Dynamics Simulation Study. *Langmuir* **2012**, *28*, 235−241.

(14) Wang, X.; Bai, H.; Shi, G. Size Fractionation of Graphene Oxide Sheets by pH-Assisted Selective Sedimentation. *J. Am. Chem. Soc.* **2011**, *133*, 6338−6342.

(15) Strong, V.; Dubin, S.; El-Kady, M. F.; Lech, A.; Wang, Y.; Weiller, B. H.; Kaner, R. B. Patterning and Electronic Tuning of Laser Scribed Graphene for Flexible All-Carbon Devices. *ACS Nano* **2012**, *6*, 1395−1403.

(16) Gilje, S.; Dubin, S.; Badakhshan, A.; Farrar, J.; Danczyk, S. A.; Kaner, R. B. Photothermal Deoxygenation of Graphene Oxide for Patterning and Distributed Ignition Applications. *Adv. Mater.* **2010**, *22*, 419−423.

(17) Abellán, G.; Coronado, E.; Martí-Gastaldo, C.; Ribera, A.; Otero, T. F. Magnetic Nanocomposites Formed by FeNi3 Nanoparticles Embedded in Graphene. Application as Supercapacitors. *Part. Part. Syst. Charact.* **2013**, *30*, 853−863.

(18) Park, S.; Lee, K.-S.; Bozoklu, G.; Cai, W.; Nguyen, S. T.; Ruoff, R. S. Graphene Oxide Papers Modified by Divalent Ions—Enhancing Mechanical Properties via Chemical Cross-Linking. *ACS Nano* **2008**, *2*, 572−578.

(19) Garcia-Gallastegui, A.; Iruretagoyena, D.; Gouvea, V.; Mokhtar, M.; Asiri, A. M.; Basahel, S. N.; Al-Thabaiti, S. A.; Alyoubi, A. O.; Chadwick, D.; Shaffer, M. S. P. Graphene Oxide as Support for Layered Double Hydroxides: Enhancing the CO2 Adsorption Capacity. *Chem. Mater.* **2012**, *24*, 4531−4539.

(20) Yoon, Y.; Lee, K.; Baik, C.; Yoo, H.; Min, M.; Park, Y.; Lee, S. M.; Lee, H. Anti-Solvent Derived Non-Stacked Reduced Graphene Oxide for High Performance Supercapacitors. *Adv. Mater.* **2013**, *25*, 4437−4444.

(21) Xiang, C.; Liu, Y.; Yin, Y.; Huang, P.; Zou, Y.; Fehse, M.; She, Z.; Xu, F.; Banerjee, D.; Hermida Merino, D.; Kraatz, H.; Brougham, D.; Wu, B.; Sun, L. A Facile Green Route to Ni/Co Oxide Nanoparticle Embedded 3D Graphitic Carbon Nanosheets for High Performance Hybrid Supercapacitor Device. *ACS Appl. Energy Mater.* **2019**, *2*, 3389−3399.

(22) Liu, L.; Liu, A.; Xu, Y.; Yu, H.; Yang, F.; Wang, J.; Zeng, Z.; Deng, S. Agglomerated Nickel−Cobalt Layered Double Hydroxide Nanosheets on Reduced Graphene Oxide Clusters as Efficient Asymmetric Supercapacitor Electrodes. *J. Mater. Res.* **2020**, *35*, 1205−1213.

(23) Wu, L.-K.; Wu, W.-Y.; Xia, J.; Cao, H.-Z.; Hou, G.-Y.; Tang, Y.-P.; Zheng, G.-Q. A Nanostructured Nickel−Cobalt Alloy with an Oxide Layer for an Efficient Oxygen Evolution Reaction. *J. Mater. Chem. A* **2017**, *5*, 10669−10677.

(24) Brousse, T.; Bélanger, D.; Long, J. W. To Be or Not to Be Pseudocapacitive? *J. Electrochem. Soc.* **2015**, *162*, A5185−A5189.

(25) Jiang, Y.; Liu, J. Definitions of Pseudocapacitive Materials: A Brief Review. *Energy Environ. Mater.* **2019**, *2*, 30−37.

(26) Ke, Q.; Wang, J. Graphene-Based Materials for Supercapacitor Electrodes — a Review. *J. Materiomics* **2016**, *2*, 37−54.

(27) Chatterjee, D. P.; Nandi, A. K. A Review on the Recent Advances in Hybrid Supercapacitors. *J. Mater. Chem. A* **2021**, *9*, 15880−15918.

(28) Zhang, S.; Pan, N. Supercapacitors Performance Evaluation. *Adv. Energy Mater.* **2015**, *5*, 1401401.

(29) Babu, B.; Simon, P.; Balducci, A. Fast Charging Materials for High Power Applications. *Adv. Energy Mater.* **2020**, *10*, 2001128.

(30) Tan, D. Z. W.; Cheng, H.; Nguyen, S. T.; Duong, H. M. Controlled Synthesis of MnO_2/CNT Nanocomposites for Supercapacitor Applications. *Mater. Technol.* **2014**, *29*, A107−A113.

(31) Kim, S. K.; Koo, H. J.; Lee, A.; Braun, P. V. Selective Wetting-Induced Micro-Electrode Patterning for Flexible Micro-Supercapacitors. *Adv. Mater.* **2014**, *26*, 5108−5112.

(32) El-Kady, M. F.; Strong, V.; Dubin, S.; Kaner, R. B. Laser Scribing of High-Performance and Flexible Graphene-Based Electrochemical Capacitors. *Science* **2012**, *335*, 1326−1330.

(33) El-Kady, M. F.; Kaner, R. B. Scalable Fabrication of High-Power Graphene Micro-Supercapacitors for Flexible and on-Chip Energy Storage. *Nat. Commun.* **2013**, *4*, 1475.

(34) Peng, Z.; Ye, R.; Mann, J. A.; Zakhidov, D.; Li, Y.; Smalley, P. R.; Lin, J.; Tour, J. M. Flexible Boron-Doped Laser-Induced Graphene Microsupercapacitors. *ACS Nano* **2015**, *9*, 5868−5875.

(35) Lin, J.; Zhang, C.; Yan, Z.; Zhu, Y.; Peng, Z.; Hauge, R. H.; Natelson, D.; Tour, J. M. 3-Dimensional Graphene Carbon Nanotube Carpet-Based Microsupercapacitors with High Electrochemical Performance. *Nano Lett.* **2013**, *13*, 72−78.

(36) Wu, Z. S.; Parvez, K.; Feng, X.; Mullen, K. Graphene-Based in-Plane Micro-Supercapacitors with High Power and Energy Densities. *Nat. Commun.* **2013**, *4*, 2487.

(37) Jung, H. Y.; Karimi, M. B.; Hahm, M. G.; Ajayan, P. M.; Jung, Y. J. Transparent, Flexible Supercapacitors from Nano-Engineered Carbon Films. *Sci. Rep.* **2012**, *2*, 773.

📖 Recommended by ACS